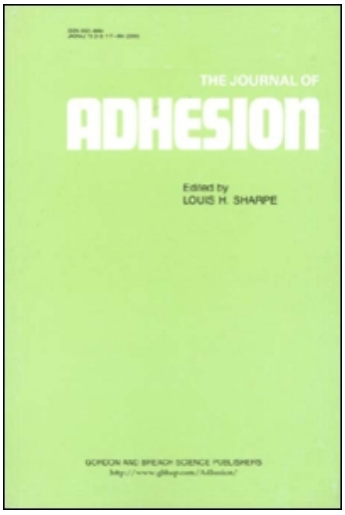

The Journal of Adhesion
Publication details, including instructions for authors and subscription information:
http://www.informaworld.com/smpp/title~content=t713453635

The Mechanisms of Peeling of Uncross-Linked Pressure Sensitive Adhesives

L. Benyahia[a]; C. Verdier[a]; J. -M. Piau[a]
[a] Laboratoire de Rhéologie, Domaine Universitaire, Grenoble, Cedex, France

To cite this Article Benyahia, L. , Verdier, C. and Piau, J. -M.(1997) 'The Mechanisms of Peeling of Uncross-Linked Pressure Sensitive Adhesives', The Journal of Adhesion, 62: 1, 45 — 73
To link to this Article: DOI: 10.1080/00218469708014562
URL: http://dx.doi.org/10.1080/00218469708014562

J. Adhesion, 1997, Vol. 62, pp. 45–73
Reprints available directly from the publisher
Photocopying permitted by license only

The Mechanisms of Peeling of Uncross-Linked Pressure Sensitive Adhesives

L. BENYAHIA, C. VERDIER and J.-M. PIAU

Laboratoire de Rhéologie, Domaine Universitaire BP53*
38041 Grenoble Cedex 9, France

(Received 17 July 1996; In final form 14 September 1996)

We analyze the peeling properties of an uncross-linked pressure sensitive adhesive. 90° peeling master curves on Pyrex™ and PMMA (polymethylmetacrylate) are constructed. The shift coefficients a_T are compared with the ones obtained from rheometrical shear tests.

With our machine, the peeling front is kept fixed, enabling us to observe the mechanisms of deformation of the adhesive. We count four different mechanisms of peeling in cohesive failure, and three in interfacial peeling (the last being unstable); they correspond to various slopes that we identify. The flow patterns at slow reduced velocities are two-dimensional. Then they undergo transitions to three-dimensional periodic complex flows, due to instabilities in the flow of thin adhesives. Interpretation of these peeling master curves are discussed in terms of rheology and physico-chemistry. It appears necessary to take into account the elongational properties of the adhesive, as well as the surface energy properties, to predict adhesion.

Keywords: Adhesion; rheology; polymer; pressure sensitive adhesive; peel; mechanisms; cohesive; interfacial; contact angle

1. INTRODUCTION

In this paper, we study pressure sensitive adhesives (P.S.A), which are widely used materials in modern industry (packaging, release coatings, labels, hospital products...). Many studies have been undertaken to understand the adhesion properties of these materials. In particular, surface energies, the rheological properties (shear moduli, glass transition

*Universités de Grenoble (UJF Grenoble I-INPG), and CNRS (UMR 5520).

temperature), adhesive thickness, backing and substrate, all play an important role when predicting the adhesive properties of a P.S.A.

There are different ways of measuring the adhesive properties [1], in particular, the peeling test is one way to do so: one pulls on a strip of adhesive coated onto a backing, to remove it from a given substrate. The force, F, necessary to separate the bond is measured as well as the velocity, V, at which the peeling front moves.

The force required in a peeling test depends both on the physico-chemical properties of the different surfaces, and on the rheology of the adhesive. Actually, one can draw peeling master curves using the time/temperature superposition principle [2, 3] when it can be applied to the rheometrical properties of the adhesive. Still, some cases have been encountered where the shift coefficients are not those of the adhesive [4].

It is generally found that there are two modes of steady failure, a cohesive one and an interfacial one. At low velocities or high temperatures, stresses within the adhesive are high enough so that the failure mode is cohesive, and the adhesive remains both on the substrate and the backing. This can give rise to comparatively very high peeling energies [3].

At moderate rates, the adhesive undergoes a transition from cohesive to interfacial failure. The interfacial mode corresponds to a flow mode where the adhesive stays on one side only (substrate or backing). In practice, the most common case is the one where the adhesive remains on the backing. The peeling energy increases with the rate of peel [5].

Many authors have tried to describe this type of peeling. It has been shown [6, 7, 8] that the peeling energy (G) required to break the bond away from the substrate (interfacial failure) is proportional to the thermodynamic work of adhesion, w

$$G = w\,\phi(a_T V) \tag{1}$$

where $a_T V$ is called the reduced velocity (a_T is a coefficient depending on temperature) and ϕ is a dimensionless function of the reduced velocity representing the dissipative energy, depending on the rheology of the adhesive. Also, the cohesive part of the curve obeys a similar relationship where one should replace w by the cohesive energy of the adhesive when in contact with a specified liquid or atmosphere [8, 9].

When the failure is interfacial at low enough velocities, the energy is of the same order as the work of adhesion, w. On the other hand, at high velocities, G can sometimes be two or three orders of magnitude higher than w.

In some cases this dissipation function has been determined to be a simple power law of the form [5, 10]

$$\phi(a_T V) = 1 + (a_T V)^n \tag{2}$$

where n is a function of the adhesive. For example, the case of separation of polyurethane [5] from glass gives $n = 0.6$.

At high peeling velocities, an instability occurs. This type of peeling is related to the rubber glass transition [3, 11, 12, 13] and an oscillatory force is observed under controlled peeling velocity, due to the combined elasticity of the backing and the adhesive.

To be able to understand the effect of rheology on the adhesive properties, one needs to find out what type of flow exists at the peeling front. The actual question is to know whether the shear or elongational effects are preponderant or both. The simplest idea is to try to conduct careful visualizations of the flow mechanisms involved. A special case [14] of peeling has been analyzed by looking at the peeling front through a Pyrex™ glass substrate, thus showing a two-dimensional picture from which the three-dimensional flow pattern was guessed. Still, no clear pictures showing the evolution of the flow regimes have been shown, as we move along the master curve.

In the present paper, the study of a 90° peeling experiment of an uncross-linked P.S.A. (containing copolymers with styrenic blocks) on two substrates (Pyrex™ and polymethylmetacrylate (PMMA) is performed. The originality of this work consists of the simultaneous interesting features:

- the measurements of peeling curves at different temperatures, under controlled humidity, in a large range of reduced velocities (eight decades)
- the visualization of the peeling front with a special system allowing magnification of the mechanisms. This enables one to see a three-dimensional picture of all the mechanisms
- complementary rheological and surface characterizations of the adhesive and substrate, respectively

In section 2, we present the experimental set-up, as well as the information concerning the materials and the testing procedures. The peeling experiment built in our Laboratory is described, along with the observation system used.

Then we show the evolution of the mechanisms in relation to peeling master curves (on Pyrex™ and PMMA), in a large range of reduced velocities (section 3). The construction of the peeling master curve allows the determination of the shift factors a_T to be compared with the ones obtained from dynamic shear rheometry.

The photographs taken from the peeling front are crucial for the understanding of the problem and show clearly that there are various modes of flow in cohesive failure, as well as in interfacial failure. In both cases, the flow is first two-dimensional, then a transition occurs, corresponding to a hydrodynamic instability, and the flow becomes three-dimensional. This instability in cohesive failure is similar to the one observed for a fluid forming a free surface when driven by two rotating rollers [15, 16, 17]. Furthermore, we have counted four mechanisms in the cohesive mode of peeling and three when the peeling is interfacial.

This is the first time that all mechanisms characterizing the 90° peeling of an uncross-linked adhesive are provided, in close relation to peeling master curves. This study is very helpful for modeling the flow at the peeling front, which governs the peeling force, and for deriving scaling laws corresponding to each flow regime.

2. EXPERIMENTAL DETAILS

Material and Preparation of Adhesive Strips

The adhesive used throughout this study is intended to be used in pharmaceutical application. It is an uncross-linked H.M.P.S.A. (Hot Melt Pressure Sensitive Adhesive). It contains about 20% of a copolymer (with styrenic blocks), 40% of tackifiers and additional plasticizers (waxes). The copolymer contains about 70% of triblock compound and 30% of diblock compound. The role of the tackifier is to increase the glass transition temperature T_g (this has been verified by separate dynamic measurements), and the adding of non-crystalline compatible plasticizers adjusts the plateau modulus of the mixture. In

this case, T_g is approximately equal to $-25°C$ (measured dynamically, $f = 1$ Hz) and the melt temperature is $T_m = 45°C$.

The adhesive tape has a 100 μm thickness. It is coated over a 23 μm-thick rigid (but flexible) polyester backing (Hoechst, RN 23, Young Modulus $E = 4500$ MPa) at a temperature of 110°C and the coating rate is 2m/min. The other side of the adhesive is protected by a siliconed polyester sheet (Rexor, 74 H, thickness 75 μm) which is moved away clean from the P.S.A. just before applying the adhesive on the substrate. For the peeling test, 300 × 30 mm strips are cut from the sheet.

Rheological Measurements

Dynamic rheological measurements were carried out on a Carrimed CS 100 rheometer, using a cone and plate geometry (radius = 20 mm, angle = 4°). The deformation measurement for low enough controlled stress values at various frequencies allows the determination of the storage modulus (G') and the loss modulus (G''), as functions of the frequency ($f = \omega/2\pi$, 10^{-2} Hz $\leqslant f \leqslant 10$ Hz). Measurements were carried out at five temperatures (0°C, 20°C, 35°C, 50°C). It is found that the time-temperature superposition principle can be applied to the adhesive and shift factors a'_T are determined by translation of the curves obtained at the different temperatures onto the reference curve ($T_{ref} = 35°C$). This is shown in Figure 1.

Preparation of Substrates

In this study we used two substrates: Pyrex™ and PMMA. Kaelble [3] and later Gent and Schultz [6] have demonstrated the importance of the surface energies both of the adhesive and of the substrate on the peeling behavior. Thus, the substrates are cleaned using a defined protocol which produces a clean and reproducible surface. The adhesive is then applied on the latter surface under controlled pressure. The cleaning of the substrate not only allows one to improve the repeatability of the measurements but also reduces the waiting time.

First the Pyrex™ substrate (roughness $Ra = 0.0025$ μm) is washed with acetone in order to eliminate most of the pollution (grease, water,...) present at the substrate interface. The Pyrex™ substrate is

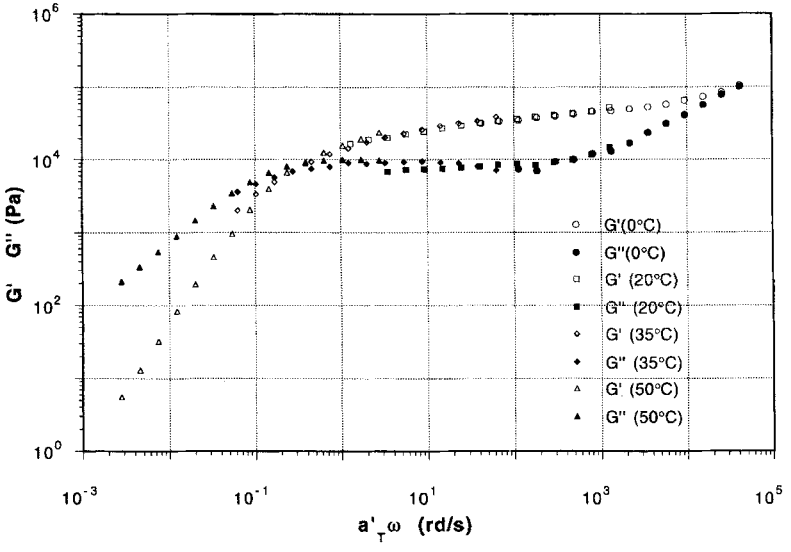

FIGURE 1 Dynamic shear moduli G' and G'' ($T_{ref} = 35°C$).

then put into a sulfochromic-acid solution. This treatment is similar to the one described in the case of steel [18]. The substrate is free of all sorts of pollution. In the end, the Pyrex™ is rinsed with distilled water and dried in a vacuum oven at 50°C for 10 min.

The PMMA substrate (roughness $Ra = 0.01\ \mu m$) is cleaned first using ethyl alcohol. Then the substrate is put into an ultrasonic bath containing Freon TF. Finally, the PMMA is dried in a vacuum oven (pressure 10 mm Hg) at 50°C for 10 min.

Surface Energy Measurements

The sessile drop method is used to measure the contact angles between five wetting liquids and the different surfaces (substrates, polyester backing and adhesive). The same cleaning protocol used for the PMMA is applied for the polyester backing. An approximation due to Fowkes [19] and later extended by Owens *et al.* [20] is chosen to calculate the surface free energy. The surface free energy, γ, is divided into two components, γ^d and γ^p, which refer,

respectively, to the contribution of the dispersive and polar forces

$$\gamma = \gamma^d + \gamma^p \tag{3}$$

Then the adhesion energy, w_{sl}, between a given solid (s) and the wetting liquid (l) can be expressed by

$$w_{sl} = \gamma_s + \gamma_l - \gamma_{sl} = \gamma_l(1 + \cos\theta) \tag{4}$$

after using Young's equation. In Eq. (3), γ_s and γ_l denote, respectively, the surface free energies of the solid and the liquid. θ is the angle between the drop and the solid, measured with a contact angle-meter (Face, CA-A). γ_{sl} is the interfacial free energy between the solid and the liquid.

Following the method developed in Refs. 19, 20, we introduce the dispersive and polar components and assume that

$$\gamma_{sl} \approx \gamma_s + \gamma_l - 2(\gamma_s^d \gamma_l^d)^{1/2} - 2(\gamma_s^p \gamma_l^p)^{1/2} \tag{5}$$

Finally the combination of Eqns. (4) and (5) leads to:

$$\frac{\gamma_l(1+\cos\theta)}{2(\gamma_l^d)^{1/2}} = (\gamma_s^d)^{1/2} + (\gamma_s^p)^{1/2}\frac{(\gamma_l^p)^{1/2}}{(\gamma_l^d)^{1/2}} \tag{6}$$

A plot of $\gamma_l(1+\cos\theta)/2(\gamma_l^d)^{1/2}$ as a function of $(\gamma_l^p)^{1/2}/(\gamma_l^d)^{1/2}$ for known liquids allows one to draw a straight line whose ordinate for zero abscissa and slope give access respectively to the dispersive and polar components of the surface free energy of the given solid (γ_s). Table I shows the different values of the surface free energies obtained in our case.

TABLE I Polar and dispersive components of surface free energies

Solid	γ^d (mJ/m^2)	γ^p (mJ/m^2)	γ (mJ/m^2)
Pyrex™	34.6 ± 1.1	30.2 ± 2.0	64.8 ± 3.1
PMMA	45 ± 1.4	0.2 ± 0.5	45.2 ± 1.9
Adhesive	38.8 ± 1.2	0 ± 0.5	38.8 ± 1.7
Polyester	42 ± 1.6	2.3 ± 1.2	44.3 ± 2.8

We further note that since the adhesive contains mostly C—H bonds, the main forces should give rise to non polar components of the surface free energy, which is the case ($\gamma^p = 0$). Due to the uncertainty of such measurements (advancing and receding angles may give different values, also roughness may alter the precision), we have added the measurement error. Therefore, in the case of PMMA and Polyester, the comparison is difficult. The γ_d component, though, gives more accurate information because it was obtained using a purely dispersive fluid.

Peeling Apparatus

The peeling apparatus is composed of two micrometric tables (Microcontrôle, MT 160) driven by two step-by-step motors (two configurations: UE 72 PP and UE 72 PP with a 1/50 gear ratio). A description of the apparatus is shown in Figure 2. In this configuration the peeling angle is 90°. The two tables are translated with constant and equal velocities, V. The adhesive is placed on the substrate and the latter moves horizontally, while the other part of the adhesive moves vertically pulled by the other micrometric table. Thus,

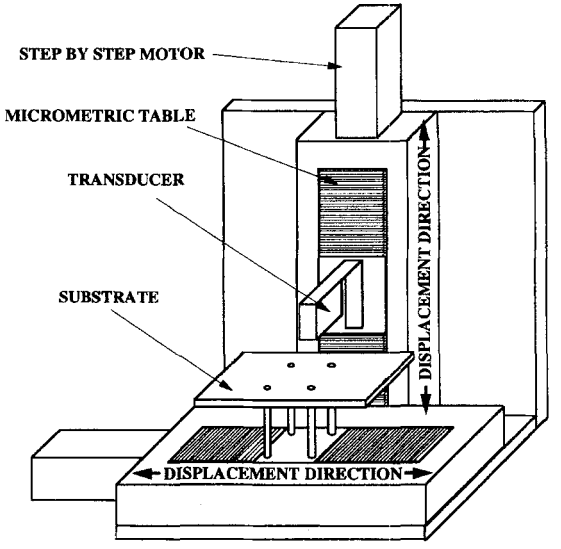

FIGURE 2 Peeling Apparatus.

the separation front is fixed in the laboratory reference frame. The adhesive is attached to the micrometric table through a force transducer (Sedeme Kistler, model XF 2, measurement range: ± 2 daN), which measures the peeling force, F.

Observation System

The peeling front is observed using a video system. A CCD black and white video-camera (SONY, SSC-M370CE) is placed in different positions with respect to the adhesive/substrate separation front. Figure 3 shows the position of the camera and the light source in a particular visualization position. The camera is placed on an articulated arm which allows different positions in space. The video signal is recorded on a U-MATIC VCR (SONY, VO-9600H). The high performance of the camera (resolution, sensitivity and available shutter speeds up to 1/10000 s), the lens (150 mm Macro-Nikkor) and the VCR (resolution) allow us to obtain excellent views of the peeling mechanisms. Storage of photographs from the video film is possible through a computer related to an AGFA-MATRIX system. The photographs obtained from this apparatus have the same resolution as the original film. The observation of the mechanisms at high pulling rates is obtained by

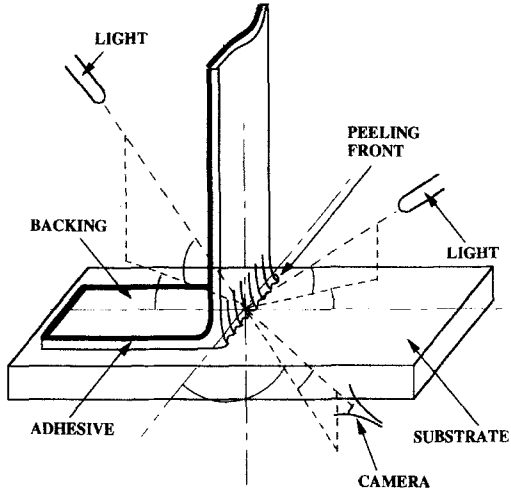

FIGURE 3 Observation System.

selecting a high value of the shutter switch available on the camera. Magnification (from 4 to 24) is achieved using prolongators with different lengths (from none up to 200 mm). The position of the camera with respect to the peeling front is obtained by adding selected focal length lenses.

The lighting of the peeling front is obtained using two optical fiber light sources. They point straight at the peeling front and their orientation is adjusted for each observation taking into account the backing curvature, the failure type and the position of the camera.

Experimental Conditions

In this study, the peeling angle is 90°. A constant pulling rate is chosen in a large range from 10^{-4} to 15 mm/s. The complete equipment is placed into a chamber under controlled temperature and humidity. Four temperatures are used (-10, 20, 35, 50°C $\pm$ 0.1°C) for the tests. Humidity is always kept at 10% R.H. ($\pm$1% R.H.). It is controlled by the measurement of the temperature difference between a humid sensor and a dry one. The minimum of humidity is selected to limit water absorption by the adhesive. This may cause swelling of the adhesive [6] and, therefore, changes in its rheology and physico-chemical properties.

Testing Procedure

When the system is set into motion at constant velocity, the force signal shows first a transient regime, then a plateau, where the force F is measured. The time required to reach the steady-state regime is inversely proportional to the pulling velocity, but it also depends on the initial conditions. The peeling energy, G(N/m), using a 90° angle is given by [21]:

$$G = \frac{F}{l} \tag{7}$$

where l is the width of the adhesive tape. The precision of this peeling energy, G, is about $\pm$5%.

3. RESULTS

When the adhesive is applied, it needs some time to flow and form chemical bonds necessary to adhere to the substrate. This contact time depends on the viscoelastic properties of the adhesive, the roughness of the substrate and the interfacial free energy of both the adhesive and the substrate. The peeling energy required to separate the adhesive from the substrate is shown in Figure 4 as a function of the contact time, for a given velocity (0.5 mm/s) and temperature (20°C). We can see that the force reaches a plateau after about thirty minutes. All peeling experiments are carried out when the peeling energy does not depend on the contact time.

3.1. Time-temperature Superposition

Figure 5 shows the cohesive peeling energy, G(N/m), *versus* the separation rate on a logarithmic diagram when the substrate is the PMMA. Figure 6 represents both the cohesive and adhesive curves using Pyrex™ as the substrate. Master curves were constructed using the method of reduced variables in both cases. Curves obtained at various temperatures

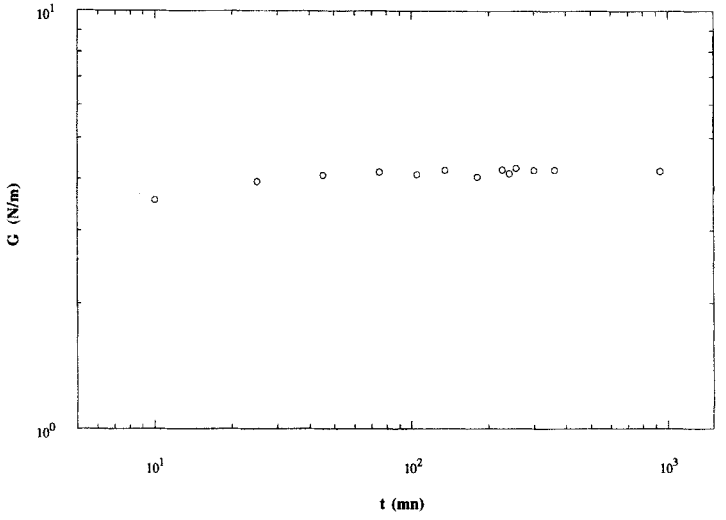

FIGURE 4 Dependence of the peeling force on the contact time (Pyrex™ $T = 20°C$, $v = 0.5$ mm/s).

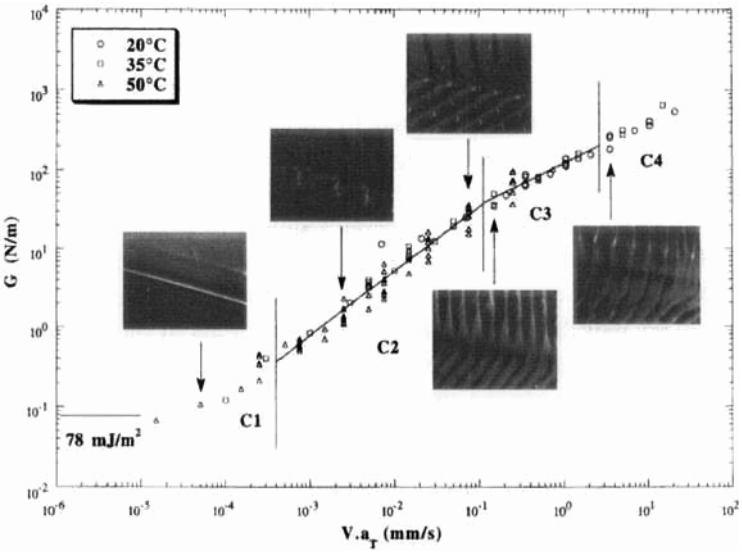

FIGURE 5 PMMA peeling master curve at $T_{ref} = 35°C$ (cohesive mechanisms).

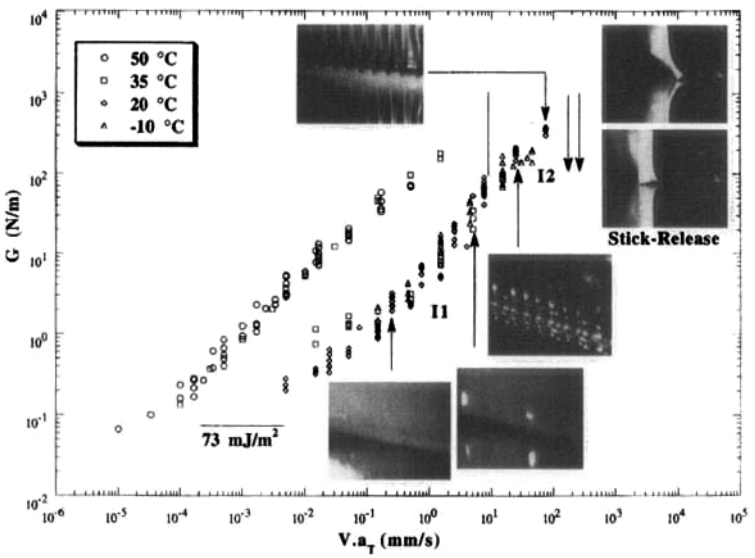

FIGURE 6 Pyrex™ peeling master curve at $T_{ref} = 35°C$ (interfacial mechanisms).

(−10, 20, 50°C) were shifted horizontally, along the rate axis, to superpose them with the curve obtained at 35°C. This temperature was chosen for application purposes. The shift factor which allows one to achieve good agreement between the curves for each temperature is called a_T. This method of master curve construction has already been applied by several authors [3, 5, 7, 13]. We did not apply the correction factor T_0/T for the vertical shift because it only creates negligible changes. Previous authors showed that the shift coefficients, a_T, obtained in peeling are comparable with those found in dynamic shearing experiments or calculated using the WLF equation. Shreuder-Stacer [4], on the other hand, shows that deviations can be obtained when peeling in different geometries. The identification of the coefficients assumes that the phenomena occurring during a peel test are simply governed by the rheological properties of the adhesive.

The shift factors obtained by shifting the peeling curves either in cohesive (*c*) or interfacial type of failure (*i*) are shown in Figure 7 in comparison with those calculated from dynamic oscillatory shear experiments (a'_T). The WLF equation has been used for fit of a'_T. The polyester does not have any influence on the peeling energy because it is inextensible in the range of forces and temperatures studied. Furthermore, it is easy to

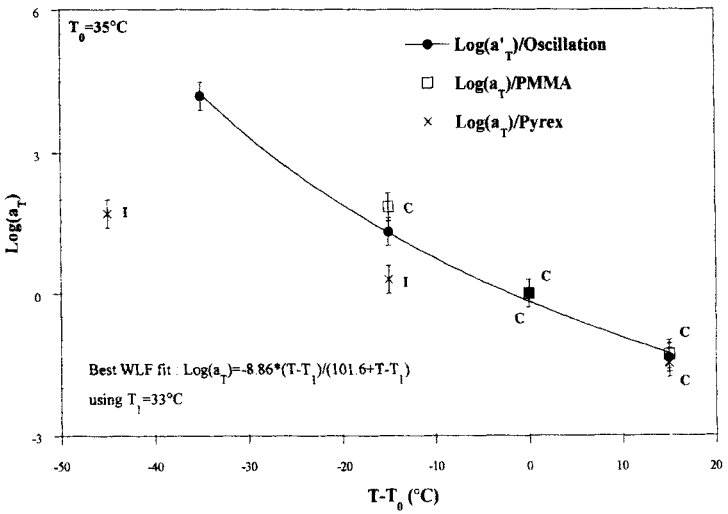

FIGURE 7 Shift factors a_T (C = cohesive, I = interfacial) and a'_T (from rheometry against $T - T_0$ ($T_0 = 35°C$) with WLF fit.

bend it, for its thickness is small. We find a good agreement between a_T and a'_T for high temperatures, when the failure is cohesive. This is true because the failure occurs within the adhesive. Thus, the behavior of the peeling joint in the cohesive regime is governed by the rheological properties of the adhesive. On the other hand, in the interfacial mode of failure, a difference is to be noted between the two factors (Pyrex™). We conclude that, for interfacial failure, one has to be careful when applying the time-temperature superposition principle. This means that adhering to a substrate may have an effect on the relaxation processes of a polymer. Indeed, it is possible that links created at the interface may change relaxation times, by reducing the chains' mobility. Another explanation may be that the failure was not completely interfacial and that there is some adhesive left on the substrate. Still we did not see any. Further investigations of the surface should be carried out in a forthcoming study. After these observations, we decided to shift our peeling curves using a_T.

3.2. 90° Peeling Mechanisms on *PMMA*: Cohesive Failure

The results of the 90° peeling curve on PMMA *versus* reduced pulling rate at different temperatures are shown in Figure 5 with the corresponding photographs for each identified mechanism.

In the present case, the failure mode is cohesive. This means that a part of the P.S.A. remains on the substrate and the rest stays with the backing after peeling.

In this particular failure mode, we can identify four different regimes of flow.

The *first mode C1* occurs at slow pulling velocity. The P.S.A. is deposited between the substrate and the backing in a two-dimensional flow pattern (Photographs 1 and 2), and the fluid lies in approximate equal amounts on both sides after peeling. The corresponding data points are not accurate enough (limiting range of the force transducer) to measure the cohesive strength of the adhesive ($w_c = 2\gamma_a \approx 78\,\text{mJ/m}^2$). Nevertheless, the order of magnitude of the energy involved is in this range. The C1 mode of cohesive flow is obtained at 50°C or at slow peeling rates. The dynamic oscillatory curve of the adhesive obtained at 50°C (Fig. 1) shows a Newtonian behavior of the adhesive at a low frequency. The dependence of the peeling energy,

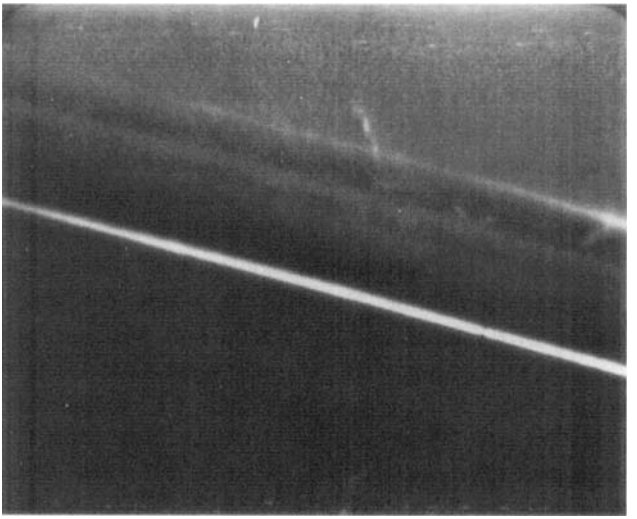

PHOTOGRAPH 1 PMMA, $T = 50°C$, $v = 0.003$ mm/s (C1) Cohesive flow regime, front view.

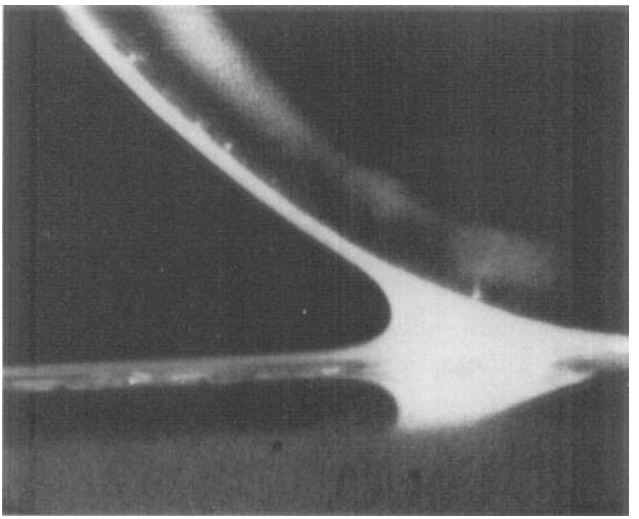

PHOTOGRAPH 2 PMMA, $T = 50°C$, $v = 0.003$ mm/s (C1) Cohesive flow regime, side view.

$G(V)$, on the dynamic moduli, $G^*(\omega)$, has been used by Komornicki *et al.* [22] to describe the peeling types of failure. It is more precisely explained in Aubrey's paper [23]. He suggests the use of a constant shift, $V = \lambda_0\omega/2\pi$, and the plotting of the two curves of $G(\lambda_0\omega/2\pi)$ and $G^*(\omega)$ on the same axis. λ_0 should correspond to the half wave that can be measured on the backing of the adhesive behind the peeling front using optical techniques. λ_0 was found to be a constant (0.6 mm) in a large range of velocities. Another way to relate these curves would be to compare a shear rate, V/e, with the angular frequency, ω. We note that $\lambda_0 \approx 0.6$ mm, so that $\lambda_0/2\pi \approx 0.1$ mm, whereas $e = 1.0$ mm. Therefore, the multiplying factor is roughly the same. Using either of the two methods, we find that the regime C1 corresponds to the Newtonian behavior of the adhesive, *i.e.* the region where G' and G'' have respective slopes of 2 and 1 (example: 10^{-3} rad/s <---> 10^{-4} mm/s).

When we increase the pulling velocity at 50°C, a three-dimensional instability occurs at the peeling front. The P.S.A. flows between the substrate and the backing and forms transparent ribs. This is the second *mode of cohesive failure C2* (Photographs 3 and 4). The same phenomenon is also observed between two rotating rollers submerged in a liquid [15, 16, 17]. The hydrodynamic instability occurs to modify

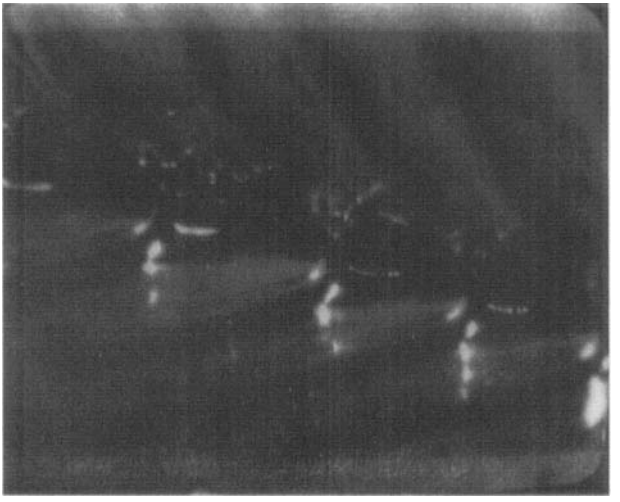

PHOTOGRAPH 3 PMMA, $T = 50$°C, $v = 0.015$ mm/s (C2) Cohesive flow regime.

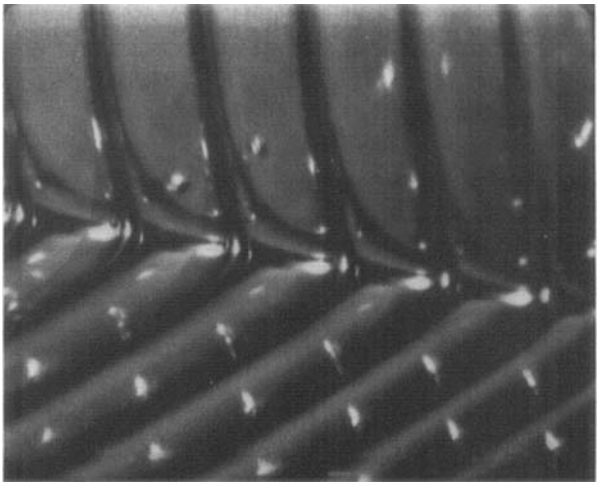

PHOTOGRAPH 4 PMMA, $T = 50°C$, $v = 1.5$ mm/s (C2) Cohesive flow regime.

the two-dimensional flow into a three-dimensional one with the appearance of ribs at a critical velocity. The same mode of flow is also observed at the low peeling rates at 35°C. The corresponding points of this second mode of flow align with a slope of about 0.8. Thus, the appearance of ribs increases the slope of the energy curve and is in close relationship with the experimental parameters. In this region of flow, the adhesive still exhibits a Newtonian behavior as shown again by the correspondence between Figures 1 and 5 (example: 10^{-1} rad/s $<---> 10^{-2}$ mm/s).

If we increase the pulling rate, the ribs become opaque and start to tear at the very edge of the free surface (Photograph 5). This third mode of *cohesive flow C3* corresponds to a slope of roughly 0.6. This mode of flow is observed at 35°C at high peeling rates as well as at 20°C and low peeling rates. The adhesive shows a rubber-like behavior (example: 10^{1} rad/s $<---> 10^{0}$ mm/s) and the mechanisms at the edge of the ribs correspond to the tearing of a rubber when subjected to an elongational test.

For the last mode of *cohesive failure C4* detected when peeling on PMMA, we have obtained a few points corresponding to a fourth mechanism. The ribs still remain opaque and there are secondary ribs peeling from the main ones (Photograph 6). This last mode of cohesive

failure is observed at 20°C. These points correspond to the rubbery behavior of the adhesive (example: 10^2 rad/s <---> 10^1 mm/s). The appearance of secondary ribs has also been observed by Urahama [14] but for interfacial failure.

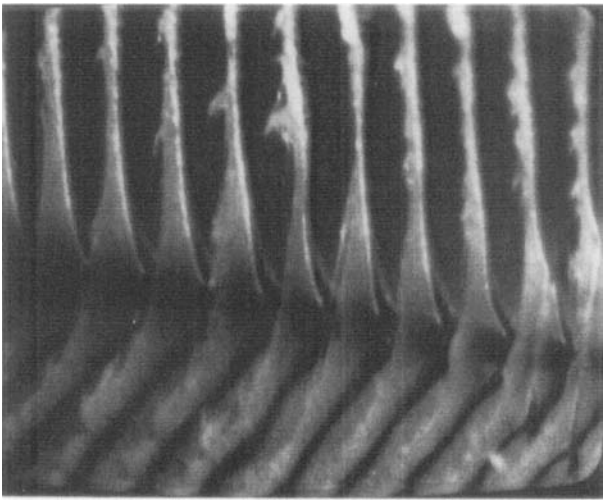

PHOTOGRAPH 5 PMMA, $T = 35°C$, $v = 0.15$ mm/s (C3) Cohesive flow regime.

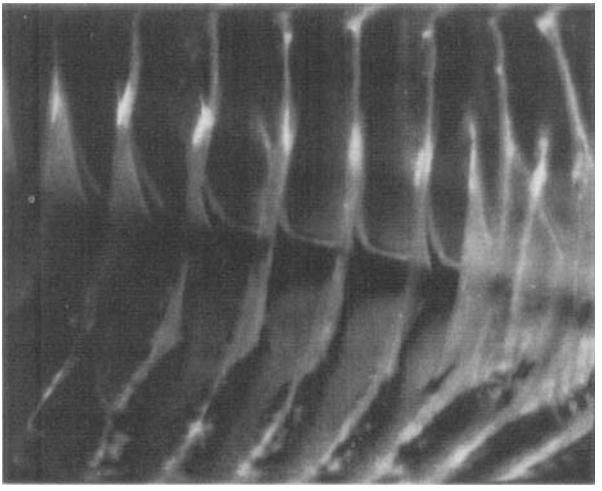

PHOTOGRAPH 6 PMMA, $T = 20°C$, $v = 0.15$ mm/s (C4) Cohesive flow regime.

This investigation of the stringiness of peeling phenomena in comparison with the rheological behavior of the adhesive confirms that a relationship exists between the behavior of the P.S.A. in cohesive failure and the rheological properties of the adhesive.

The superposition of the curves (at $T_{ref} = 35°C$) obtained at different temperatures show the superposition of the mechanisms. The points obtained at one temperature corresponding to one type of flow are in good agreement with the points corresponding to the same mechanism at another temperature. This is another reason to believe that we can apply the time/temperature superposition to a peeling process. The comparison of the characteristic dimensions, λ (wavelength) and L (height), of the ribs in cohesive failure (Fig. 8) show that for two points superposing on the master curve and corresponding to different temperatures, the dimensions of the ribs can be different. The mechanisms are similar, but the length scale is different.

From the observation of the rib's dimensions, we can say the following:

- In mole C1, λ and L and not defined.
- For the second mode, C2, when the ribs appear, λ decreases rapidly from 1.4. mm to reach a constant value (as in Ref. 15) of 0.7 mm, whereas L increases from 0.2 mm to 1.5 mm.
- The wavelength, λ, of the third mode, C3, and the fourth one, C4, does not change and equals approximately 0.3 mm. L is also a constant of 1 mm.

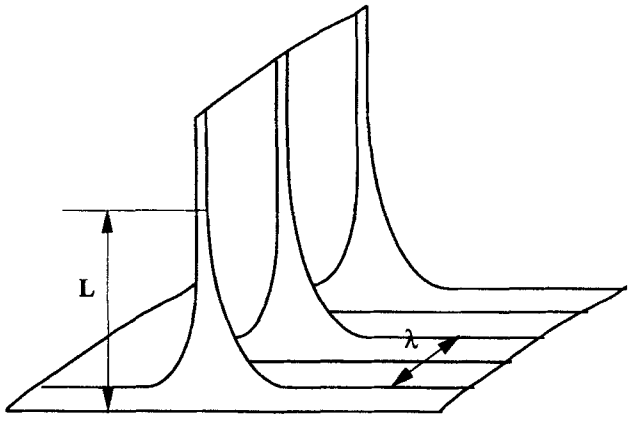

FIGURE 8 Dimensions of the rib's.

These comments and observations (shape of the free surface, wavelength...) should be very useful for further theoretical investigation of the problem, especially since most of the energy seems to be lost in these mechanisms. Indeed, a first series of investigations of the shape of the backing, using an optical technique, reveals that the crests and troughs on the backing side correspond respectively to the troughs and ribs on the adhesive. These results should appear in a forthcoming paper.

3.3. 90° Peeling on *Pyrex™*: Cohesive and Interfacial Failure

The results of peeling on Pyrex™ are shown in Figure 6. The master curve presents three modes of failure: cohesive, interfacial and an unstable region at high peeling rates. The construction of the master curve is obtained with the same method of shifting as in the PMMA case. The interfacial failure occurs at the P.S.A./substrate interface, unlike in the case of PMMA. For PMMA, we were only able to obtain interfacial failure at the interface between the backing and the adhesive. The difference in the locus of failure can be understood by comparing the reversible work of adhesion, w, between the different couples (adhesive/substrate and adhesive/backing), for the two different substrates.

The reversible work of adhesion, w, between the adhesive and the substrate (or backing), is given as in Eq. (4) by the following expression:

$$w = \gamma_a + \gamma_s - \gamma_{as} \tag{8}$$

where γ_a, γ_s, are, respectively, the surface free energies of the adhesive and the substrate (or backing), and γ_{as} is the interfacial free energy between the adhesive and the substrate (backing).

An approximation for γ_{as} similar to the one in Eq. (5) is used:

$$\gamma_{as} \approx \gamma_a + \gamma_s - 2(\gamma_a^d \gamma_s^d)^{1/2} - 2(\gamma_a^p \gamma_s^p)^{1/2} \tag{9}$$

As the polar component of the adhesive's surface free energy is zero (see Tab. I), the expression of w is simply given by:

$$w \approx 2(\gamma_a^d \gamma_s^d)^{1/2} \tag{10}$$

The values of γ^d are shown in Table II and w is calculated for the different pairs of adhesive/surface:

TABLE II Dispersive component, γ^d, and reversible work of adhesion, w, between the adhesive and the surface at $T = 20°C$

Surface	$\gamma^d\,(mJ/m^2)$	$w\,(mJ/m^2)$
PMMA	45 ± 1.4	83.6 ± 2.6
Pyrex	34.6 ± 1.1	73.3 ± 2.3
Polyester	42 ± 1.6	80.7 ± 2.5

The approximate classification is obtained:

$$w(\text{Adhesive/PMMA}) \geqslant w(\text{Adhesive/Polyester}) > w(\text{Adhesive/Pyrex}^{TM}) \tag{11}$$

These data have been obtained at 20°C and many vary with temperature; therefore, conclusions should be drawn carefully. Usually, the surface free energy decreases with temperature, so combined values will decrease, but not necessarily by the some amount.

Failure occurs at the interface where the work of adhesion is the lowest [13] (or when the dispersive part of the surface free energy is lower) because stresses need not be so large. Thus, the interfacial failure is located at the backing interface in the case of peeling on PMMA, and at the substrate interface when peeling on Pyrex™.

Mechanisms observed in cohesive failure on Pyrex™ are identical to those observed on the PMMA substrate except for the fourth mode, C4, which does not appear. Indeed, on a PMMA substrate, we have a higher work of adhesion, w, which allows us still to peel cohesively at higher reduced velocities. The stresses in the adhesive become larger, because the competition between the surface free energies required to break the bond are similar. Therefore, the adhesive undergoes a cohesive failure at higher velocities.

The interpretation of the cohesive-interfacial transition in terms of cohesive strength of the P.S.A. [23] is not sufficient. Indeed, we have observed interfacial failure on a Pyrex™ substrate and cohesive failure on the PMMA substrate at the same reduced velocity. Thus, the transition from cohesive to interfacial failure is clearly influenced by surface free energies. Actually, we expect the detachment conditions to be influenced both by the rheology (velocity, viscosity, temperature, ...) and

the surface free energies, as in the case of wetting of a surface by a liquid drop [24]. In this case, at small advancing angles, the velocity of the drop depends on the viscosity, the velocity and the surface free energies. A failure criterion has to be used (limit stress, etc.) to predict what really happens at the detachment point. We may consider that, as in Ref. 24, the governing parameters are γ_a, γ_s, γ_{as}, γ_b (surface free energy of the backing), the reduced velocity, $a_T V$, the zero-shear viscosity η_0, a characteristic relaxation time, λ_1, and the adhesive thickness, e. They can be introduced through the following dimensionless groups $\frac{V\lambda_1}{e}$, $\frac{\gamma_a}{\eta_0 V}$, $\frac{\gamma_b}{\gamma_a}$, $\frac{\gamma_s}{\gamma_a}$, $\frac{\gamma_{as}}{\gamma_a}$ (Weissenberg number, capillary number, and surface free energy ratios). For one type of adhesive, one backing, on a given substrate, the condition depends only on the capillary number, $C_a = \frac{\gamma_a}{\eta_0 V}$. As a first try, we can say that when the viscous forces are large enough compared with the surface forces, a transition will occur. This corresponds to a critical capillary number, $C_a{}^*$, and a critical velocity $V^* = \frac{\gamma_a}{C_a{}^* \eta_0}$. This shows also that, when the temperature changes, the critical velocity V^* (or $a_T V^*$) will change. Further studies with more adhesives and substrates still need to be carried out to predict this transition condition accurately.

The mechanisms observed in interfacial failure present three modes of flow. The first one is a two-dimensional mode of flow. The second kind is a three-dimensional one.

In the *first mode of flow I1*, the adhesive remains on the backing. The flow of the adhesive is two-dimensional (Photographs 7 and 8). From the pictures of the peeling front, we can observe that the height of the front increases with peeling velocity. At very low velocity, the curve can be extrapolated to a plateau where the measured peeling energy should correspond approximately to the reversible work of adhesion between the substrate and the adhesive ($w \approx 73$ mJ/m^2). This confirms the fact that the peeling energy is strongly influenced by the surface free energies of the adhesive and the substrate at low velocities [5]. The comparison of the rheometric and the peeling curves shows that this regime corresponds to the Newtonian-to-rubber transition of the adhesive. We note that two different forces can be observed for the same velocity, but at different temperatures. This is due to the fact that the transition from cohesive to interfacial failure depends, in a complicated manner, on the surface free energies, as well as the temperature and the rheology of the adhesive. This has also been observed by Obori *et al.*

[25] when varying the velocity continuously. They obtained a hysteresis loop when increasing the velocity and then decreasing it. Higher levels of forces are obtained when V goes up, whereas lower levels, corresponding to the steady-state values, are found when decreasing the velocity.

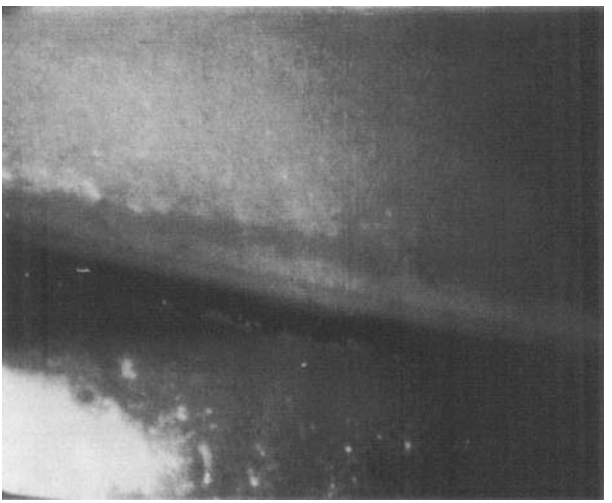

PHOTOGRAPH 7 Pyrex™, $T = 20°C$, $v = 0.05$ mm/s (I1) Interfacial flow regime.

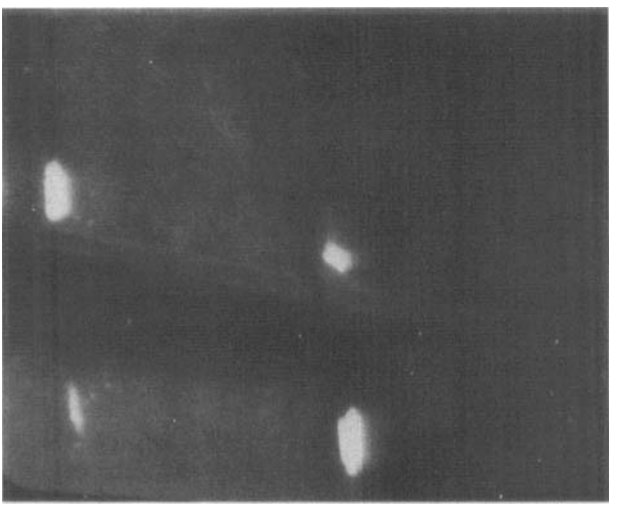

PHOTOGRAPH 8 Pyrex™, $T = -10°C$, $v = 0.05$ mm/s (I1) Interfacial flow regime.

At high peeling velocities, a hydrodynamic instability occurs and a *three-dimensional flow I2* takes place at the peeling front. The stringiness observed (Photographs 9 and 10) is similar to the one mentioned by Urahama [14] for interfacial peeling of an uncross-linked adhesive.

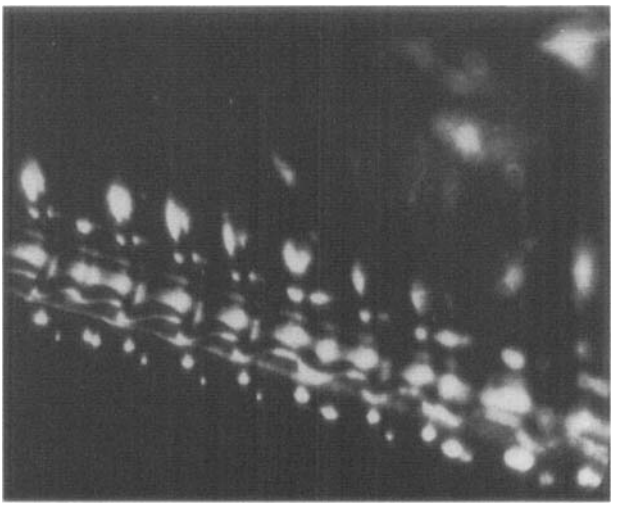

PHOTOGRAPH 9 Pyrex™, $T = 20°C$, $v = 5$ mm/s (I2) Interfacial flow regime.

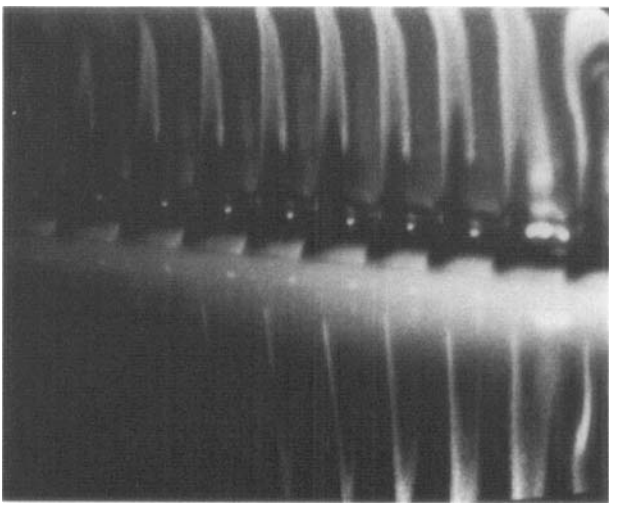

PHOTOGRAPH 10 Pyrex™, $T = 20°C$, $v = 1.5$ mm/s (I2) Interfacial flow regime.

The wavelength of the stringiness decreases with peeling rate until it reaches a constant value of 0.2 mm. The height of the filaments is approximately constant (0.5 mm) for the range of reduced velocities (10^1–10^2 mm/s) at which the stringiness shows up. The appearance of this flow is followed by a change in the curvature of the peeling master curve. The points corresponding to this regime begin to form a plateau at high velocities. The appearance of this mechanism, with regard to the shear oscillatory master curve, coincides with the rubbery behavior of the adhesive.

If we increase the velocity again, or if we decrease the temperature, *an oscillatory regime* of peeling force is obtained, corresponding to an unstable regime. This is shown in Photographs 11–12. The adhesive is submitted to a very high deformation while still adhering to the substrate (Photograph 11), until the bonds with the substrate break with a crack propagating (Photograph 12): the energy stored in the adhesive becomes too high and is then released. The velocity of propagation of the crack is larger than the peeling velocity, that is why no stable regime is possible. If we could get as high as this velocity of propagation, we could reach a stable regime. Several authors call this phenomenon a stick-slip failure, but it is clear that there is no slip here. We would rather call it "stick-release" mechanism.

To summarize these results, we sketch the type of flow occurring at the peeling front in two cases (cohesive and interfacial failure). This is

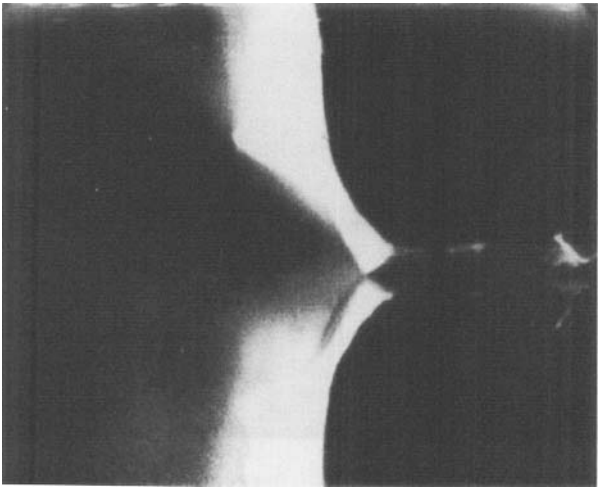

PHOTOGRAPH 11 Pyrex™, $T = -10°C$, $v = 3.5$ mm/s: Unstable regime.

shown in Figures 9a and 9b, where the steamlines are represented in a two-dimensional case. In Figure 9a, we notice the presence of a stagnation point. In Figure 9b, the detachment point is a singularity. This picture could also hold for the case of the flow within thin ribs or filaments. We conclude that, in both cases, the flow can be considered, at least in the vicinity of the stagnation point (Fig. 9a) or the detachment point (Fig. 9b), to be similar to an elongational flow of the type $u_1 = \dot{\varepsilon} x_1, u_2 = -\dot{\varepsilon} x_2, u_3 = 0$, in a reference frame $(Ox_1 x_2 x_3)$. In the case of cohesive failure, direction 1 is the dividing streamline, and direction 2 corresponds to the free surface line. In the adhesive case, direction 1 is the substrate line, whereas direction 2 is again the line following the free surface. Detachment and stagnation points are the origins O in each case.

This leads one to conclude that the mechanisms show the importance of elongational effects in 90° peeling of an adhesive. These results should be enhanced by actual quantitative predictions in a forthcoming paper.

This adhesive has enabled us to follow the evolution of a peeling master curve, and to determine the associated flow regimes.

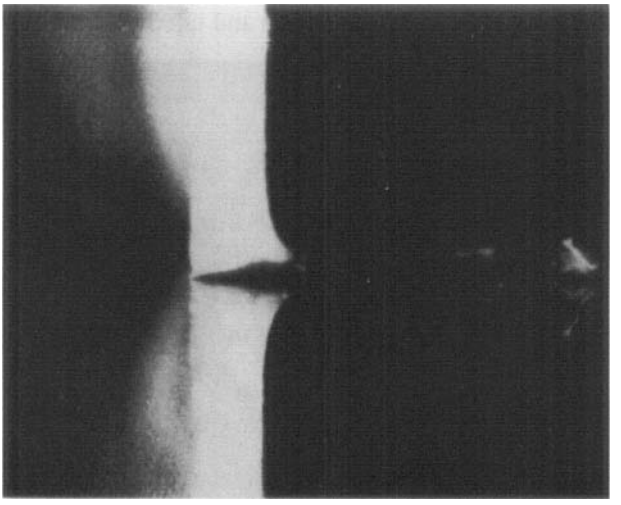

PHOTOGRAPH 12 Pyrex™, $T = -10°C$, $v = 3.5$ mm/s: Unstable regime.

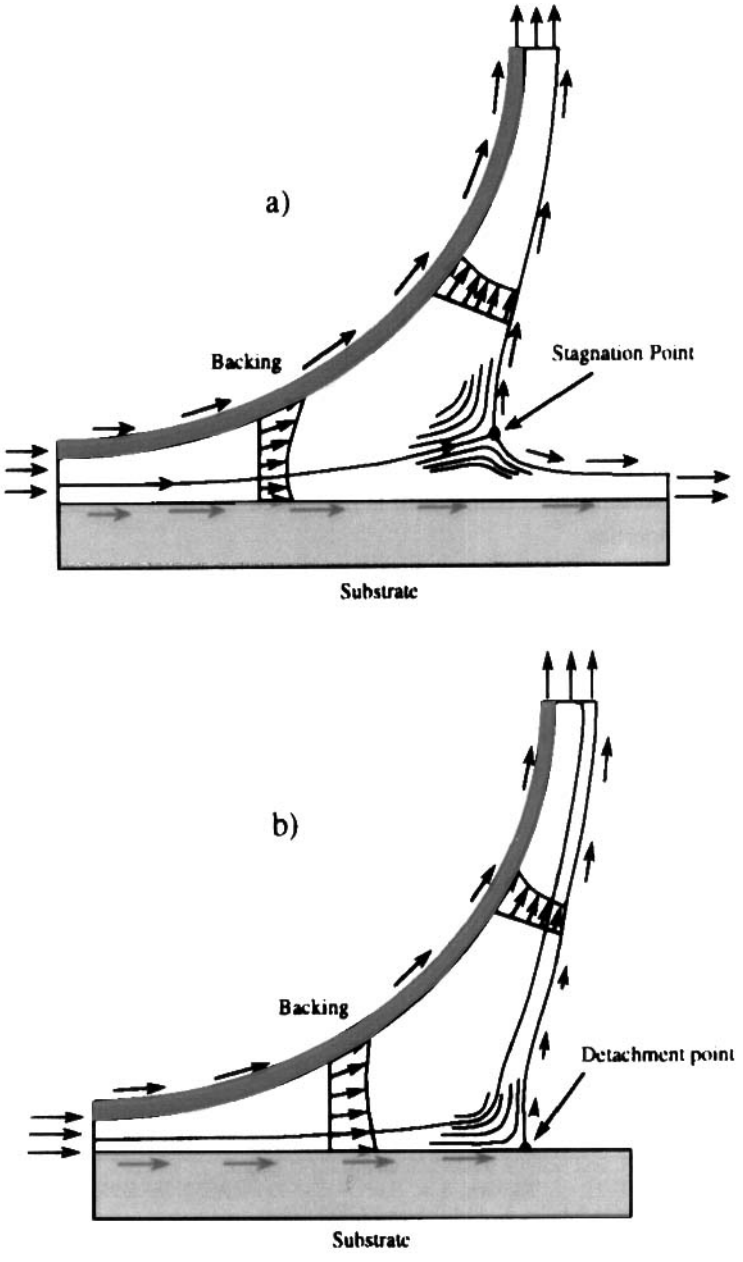

FIGURE 9 Picture of the streamlines a) cohesive mode of failure, b) interfacial mode of failure.

CONCLUSION

The whole 90° peeling master curve of an uncross-linked adhesive has been described over eight decades of reduced velocity, ranging from low velocities corresponding to Newtonian behavior, to high ones corresponding to the glassy transition of the adhesive.

The different mechanisms have been identified in correlation with the peeling master curve, for the two modes of failure: cohesive and interfacial. It has been shown that the change from one mechanism to another corresponds to changes in slopes in the peeling curves. Hence, there are several scaling laws describing the different parts of the curve.

The rheological properties are strongly coupled with the interfacial ones, especially in interfacial mode of failure. The transition from cohesive to interfacial failure also is influenced by the combination of these properties.

The shape of the peeling curves remains to be explained quantitatively, but we have shown here the importance of the elongational properties of the adhesive, which should be put into the model.

Acknowledgments

We are grateful to the Laboratories Fournier company for its financial help throughout this project, for sponsoring the thesis work of L. Benyahia, and for providing us with the adhesives.

References

[1] Satas, D., in *Handbook of pressure sensitive adhesive technology*, Satas, D., Ed. (Van Nostrand Reinhold, New York, 1989).
[2] Kaelble, D. H., *Adhesives Age* **3**, 37 (1960).
[3] Kaelble, D. H., *J. Adhesion* **1**, 102 (1969).
[4] Schreuder-Stacer, H. L., *Rubber Chem. Technol.* **61**(5), 794 (1988).
[5] Maugis, D. and Barquins, M., *J. Phys. D: Appl. Phys.* **11**, 1989 (1978).
[6] Gent, A. N. and Schultz, J., *J. Adhesion* **3**, 281 (1972).
[7] Andrews, E. H. and Kinloch, A. J., *Proc. R. Soc. Lond.* **A332**, 385 (1973).
[8] Carré, A. and Schultz, J., *J. Adhesion* **17**, 135 (1984).
[9] Schultz, J., Carré, A. and Mazeau, C., *Int. J. Adhesion and Adhesives* **4**(4), 163 (1984).
[10] Prentice, P., Proc. IXth Intl. Congress on Rheology, Mexico, 97 (1984).
[11] Barquins, M. and Pouchelon, A., *Caoutchoucs et Plastiques* **676**, 105 (1988).
[12] Aubrey, D. W. and Sherriff, M., *J. of Polym. Sci.: Polym. Chem. Ed.* **18**, 2597 (1980).

[13] Gent, A. N. and Petrich, R. P., *Proc. Roy. Soc.* **A310**, 433 (1969).
[14] Urahama, Y., *J. Adhesion* **31**, 47 (1989).
[15] Pitts, E. and Greiller, J., *J. Fluid Mech.* **11**(1), 33 (1961).
[16] Mill, C. C. and South, G. R., *J. Fluid Mech.* **28**(3), 523 (1967).
[17] Coyle, D. J., Macosko, C. W. and Scriven, L. E., *J. Fluid Mech.* **171**, 183 (1986).
[18] Bouquet, F., Cuntz, J. M. and Coddet, C., *J. Adhesion Sci. Technol.* **6**(2), 233 (1992).
[19] Fowkes, F. M., *J. Phys. Chem.* **67**, 2538 (1963).
[20] Owens, D. K. and Wendt, R. C., *J. Appl. Polym. Sci.* **13**, 1741 (1969).
[21] Kendall, K., *J. Phys. D: Appl. Phys.* **4**, 1186 (1971).
[22] Komornicki, J., Bourrel, M., Marin, G. and Brogly, M., *J. Adhesion Sci. Technol.* **6**(2), 293 (1992).
[23] Aubrey, D. W., *de nederlandse rubberindustrie* **36**(2), 1 (1975).
[24] de Gennes, P. G., *Reviews of Modern Physics* **57**(3), Part 1, 827 (1985).
[25] Obori, H., Takenaga, M., Abdulla, A. and Nakamura, A., *J. Appl. Polym. Sci.* **53**, 993 (1994).